4-1-2006

Lung Circulation Modeling: Status and Prospect

Anne V. Clough
Marquette University, anne.clough@marquette.edu

Said H. Audi
Marquette University, said.audi@marquette.edu

Robert C. Molthen
Marquette University, robert.molthen@marquette.edu

Gary S. Krenz
Marquette University, gary.krenz@marquette.edu

Accepted version. Published as part of the *Proceedings of the IEEE*, Vol. 94, No. 4 (April 2006): 753 - 768. DOI.
Robert C. Molthen was affiliated with the Medical College of Wisconsin at time of publication.

Lung Circulation Modeling: Status and Prospect

A.V. Clough
Department of mathematics, Statistics and Computer Science, Marquette University
Milwaukee, WI
S.H. Audi
Department of Biomedical Engineering, Marquette University
Milwaukee, WI
R.C. Molthen
Department of Biomedical Engineering, Marquette University
Department of Medicine: Pulmonary and Critical Care, Medical College of Wisconsin
Milwaukee, WI
G.S. Krenz
Department of mathematics, Statistics and Computer Science, Marquette University
Department of Medicine, Pulmonary and Critical Care Division, Zablocki VA Medical Center
Milwaukee, WI

Abstract: Mathematical modeling has been used to interpret anatomical and physiological data obtained from metabolic and hemodynamic studies aimed at investigating structure-function relationships in the vasculature of the lung, and how these relationships are affected by lung injury and disease. The indicator dilution method was used to study the activity of redox processes within the lung. A steady-state model of the data was constructed and used to show that pulmonary endothelial cells may play an important role in reducing redox active compounds and that those reduction rates can be altered with oxidative stress induced by exposure to high oxygen environments. In addition, a morphometric model

Proceedings of the IEEE, Vol 94, No. 4 (April 2006): pg. 753-768. DOI.

of the pulmonary vasculature was described and used to detect, describe,and predict changes in vascular morphology that occur in response to chronic exposure to low-oxygen environments, a common model of pulmonary hypertension. Finally, the model was used to construct simulated circulatory networks designed to aid in evaluation of competing hypotheses regarding the relative contribution of various morphological and biomechanical changes observed with hypoxia. These examples illustrate the role of mathematical modeling in the integration of the emerging metabolic, hemodynamic, and morphometric databases.

Section I.

Introduction

The primary function of the pulmonary arterial system is to distribute blood flow in proportion to alveolar ventilation, while maintaining input impedance consistent with optimal right heart function. The function of the pulmonary capillary bed is to provide the entire output from the right heart sufficient time in close apposition to alveolar gas for essentially complete capillary blood–alveolar gas equilibration. The role of the pulmonary venous system is to conduct the capillary blood back to the heart, without excessive capillary pressure or interference with the distributing function of the pulmonary arterial system. These hemodynamic functions must be robust over the wide range of cardiac output, from rest to maximal exertion, and lung volume, from near residual volume to near total lung capacity. Lung diseases disrupt these functions by changing the architecture and mechanical properties of the pulmonary vessels and surrounding tissues. These changes can exacerbate any mismatch between local perfusion and ventilation, inefficient gas exchange, systemic hypoxemia, and can even result in pulmonary hypertension and cor pulmonale. Thus, there has been much investigation devoted to understanding structure–function relationships in the pulmonary vasculature and how these relationships are affected by physiological adaptation and lung injury and disease.[1–2,3,4,5,6,7,8,9,10,11]

Mathematical modeling has played an important role in understanding the hemodynamics of the lungs. Several deterministic models of the pulmonary vascular bed have been developed as tools for understanding the functional implications of the measured geometry and mechanical behavior of the components of the pulmonary vascular bed.[6–7,8,12,13] Generally, these models are based on principles of mass and momentum conservation that lead to the expression of the pressure-flow relationship within a vessel (Poiseuille's law), in combination with empirical data stored in a database. Recently this approach has been used to understand the implications of pulmonary disease, such as the vascular remodeling that occurs with pulmonary hypertension.

Proceedings of the IEEE, Vol 94, No. 4 (April 2006): pg. 753-768. DOI.

Besides its respiratory function, the lungs serve important nonrespiratory functions primarily due to the large capillary surface area.[14,15] These include pulmonary distribution and/or metabolism of biogenic amines,[16] lipophilic amine drugs,[17,18] angiotensin converting enzyme substrates,[19,20] redox active compounds,[14,15,21,22] and other ligands or substrates for specific receptors, transporters, or enzymes.[23,24] Indicator dilution methods for investigation and characterization of these activities, for the most part, utilize measurement of the venous outflow concentration of the compound of interest (indicator) after bolus injection or pulse infusion. More recently such studies have been undertaken using an imaging approach wherein regional distributions of the indicator can be obtained.[25,26] Studies have been carried out in a variety of animal models both *in vivo* and in isolated perfused lungs. A key component leading to novel interpretations of these studies has been development of mathematical models that estimate parameters descriptive of the dominant interactions between the indicator and lung tissue components. The studies have provided the means to quantify functional lung parameters including heterogeneity of the capillary circulation, changes in perfused surface area, and changes in the chemical and cellular composition of lung tissue, all of which can be altered by lung disease or injury. One important example under investigation is the redox status of lung tissue and its response to oxidant stress that occurs in lung injury and disease.

In this paper, we survey the current status of mathematical modeling applied to the pulmonary circulation by examining several examples of studies designed to investigate the impact of oxidative stress (either high or low levels of inspired oxygen) on lung function. The first section introduces the indicator dilution method and applies the technique to a study of redox activity within the lung, examining its change in response to hyperoxia. The analysis reveals that the distribution of blood transit times in the pulmonary microcirculation may be critical in the interpretation of the data, so the second section describes methods for evaluating the heterogeneity of transit times within the pulmonary circulation. The third section describes mathematical models that have been developed to detect, describe, and predict changes in vascular morphology that occur in response to hypoxia, a model of pulmonary hypertension, using data obtained from microfocal computed tomography (CT) images of rat lungs. Finally, the vascular morphology models and data are used as a starting point for constructing simulated circulatory networks designed to aid in evaluation of competing hypotheses regarding the relative contribution of various morphological and biomechanical changes observed with hypoxia.

Proceedings of the IEEE, Vol 94, No. 4 (April 2006): pg. 753-768. DOI.

Section II.

Indicator Dilution Method for Studying Hyperoxic Lung Injury

Indicator dilution methods are based on explaining, both qualitatively and quantitatively, how concentrations of two or more substances (indicators), usually a vascular indicator plus the substrate(s) and/or product(s) of interest, vary with time as they pass through the lung. The indicators are introduced into the lung inflow as a rapid bolus or a pulse of finite duration, and then their concentrations are measured in the venous outflow as functions of time. The information content of data resulting from indicator dilution methods can be complex because, in addition to the metabolic processes of interest occurring within the tissue, organ perfusion (e.g., capillary surface area and transit time distribution), and reactions taking place in the blood (e.g., plasma–protein binding, metabolism by enzymes, uptake, and/or binding to formed elements) can influence the amount of indicator removed and/or modified on passage through the organ. Thus, interpretation of data necessitates the use of mathematical models based on hypotheses regarding the processes responsible for the mechanisms of indicator disposition on passage through the organ.

Indicator dilution methods have been used to investigate the mechanisms involved in lung injury and adaptation during exposure of animals to high levels of inspired oxygen.[27–28,29,30] This high oxygen environment, known as hyperoxia, is a common clinical therapy, that nonetheless presents an oxidative stress that can be toxic to the lungs.[27,28,30] Thus, animal models have been developed to evaluate the time course, severity and pathophysiological mechanisms involved.[31,32] These models have revealed that increased formation of reactive oxygen species (ROS), such as superoxide and hydrogen peroxide, plays a key role in the pathogenesis of lung O_2 toxicity, and that the pulmonary endothelium is a primary site of O_2 toxicity.

The rat model of hyperoxic lung injury mimics lung O_2 toxicity observed clinically, but the rat model is unique in that animals exposed to 85% O_2 for ~5 days develop tolerance to the otherwise lethal effects of 100% O_2.[31, 33] Studies investigating the effect of hyperoxia on the activities of pro- and/or antioxidant enzyme systems using lung homogenate[31–32,33] are important because of the range of manipulations that can be achieved. However, mechanisms identified in these reduced systems need to be evaluated at the organ level to determine their quantitative significance in intact lungs. Studies evaluating cell functions in intact lungs have lagged behind the advances of *in vitro* cell biology, in part because of the complexities involved in studying multiple interacting cell

Proceedings of the IEEE, Vol 94, No. 4 (April 2006): pg. 753-768. DOI.

types within an intact functioning organ. In this section, we present an example of the use of the indicator dilution method and mathematical modeling to quantify the effect of hyperoxia (85% O_2 exposure for 21 days) on the activity of an antioxidant enzyme (NAD(P)H : quinone oxidoreductase $_1$, NQO_1) in the rat lung.

A. Duroquinone Reduction During Passage Through the Pulmonary Circulation

The redox-active compound duroquinone, DQ (2,3,5,6-tetramethyl-1,4-benzoquinone) has been used as a substrate for NQO_1.[14,15] and hence has the potential to elucidate the effects of exposure to hyperoxia on lung NQO_1 activity. As a first step, an experimental protocol was developed to identify the dominant vascular and tissue processes that affect DQ disposition on passage through the lungs of rats exposed to room air (normoxic rats).[14] The primary measurements were the pulmonary venous outflow concentrations of DQ and its reduction product, durohydroquinone (DQH_2), during arterial pulse infusion of DQ, with and without inhibitors. Fig. 1 shows the outflow concentrations of DQ, DQH_2, and the vascular indicator fluorescein isothiocyanate dextran (FITC-dex) during 60-s pulse infusions of DQ and FITC-dex in normoxic isolated perfused rat lungs. The concentrations of the various chemical species are represented as fractions of the pulmonary arterial DQ or FITC-dex concentrations ([DQ] and [FITC-dex], respectively). The [FITC-dex] outflow curve represents what the DQ curve would have been had DQ simply remained in the perfusate and not interacted with the lung as it passed through the pulmonary circulation. A large fraction of the infused DQ in the venous outflow is present as DQH_2, illustrating the ability of the lung to reduce DQ. The outflow [DQ], [DQH_2], and [FITC-dex] reached steady state by ~50 s.

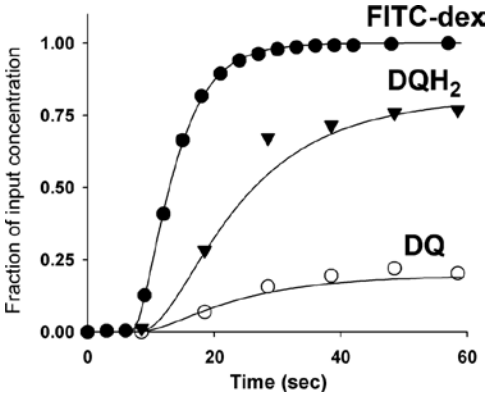

Fig. 1. Examples of the time course for the venous outflow concentrations of FITC-dex, DQ, and DQH_2 during a pulse infusion of FITC-dex or DQ into the pulmonary artery of a normoxic rat lung. The solid lines are model fits to data.

Proceedings of the IEEE, Vol 94, No. 4 (April 2006): pg. 753-768. DOI.

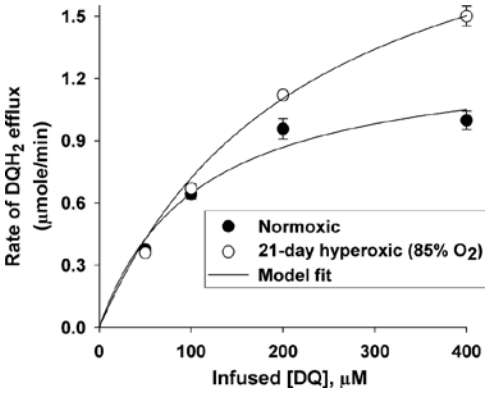

Fig. 2. Relationship between the steady-state venous outflow concentration of DQH_2 and the infused DQ concentration for normoxic (n=7) and hyperoxia lungs (n=5). Values are mean ±SE. Solid lines are model fit to the data.

The capacity of normoxic and hyperoxic lungs to reduce DQ was evaluated by varying the infused [DQ]. Fig. 2 shows the relationship between the steady-state rate of lung DQH_2 efflux during DQ infusion, defined as the product of the steady-state venous outflow [DQH_2] and perfusate flow, and the infused [DQ]. The steady-state rate of DQH2 efflux during DQ infusion was higher in hyperoxic lungs as compared to normoxic lungs during DQ infusion at 200 and 400 μM. Perfusion with dicumarol, an NQO_1 inhibitor, completely inhibited (>96%) DQH_2 efflux during infusion of the high concentration of DQ, suggesting that NQO_1 is the dominant DQ reductase in both normoxic and hyperoxic lungs.

B. Kinetic Modeling

Interpretation of the data in Figs. 1 and 2 is not straightforward, since the rate of lung DQH_2 efflux during DQ infusion is determined not only by NQO_1-mediated DQ reduction, but also by other vascular and tissue interactions. A kinetic model to interpret the data and to estimate parameters descriptive of the dominant interactions was developed.[14] Changes in these parameters form the basis for the evaluation of the effect of hyperoxia on lung NQO_1 activity.

As shown in Fig. 3, the model consists of a capillary volume (V_c) and its surrounding tissue volume (V_c). The free forms (i.e., not albumin bound) of both DQ and DQH_2 are assumed to be freely permeable into V_e.[14] Within V_c, the model allows for nonspecific rapidly equilibrating interactions of DQ and DQH_2 with the albumin perfusate P_c. Within V_e, two-electron DQ reduction to DQH_2, DQH_2 oxidation to DQ, and nonspecific rapidly equilibrating interactions of DQ and DQH_2 with lung tissue sites of association P_c are permitted. EH and E^+ are the reduced and oxidized forms, respectively, of intracellular

Proceedings of the IEEE, Vol 94, No. 4 (April 2006): pg. 753-768. DOI.

electron donor(s). The reduction of DQ to DQH_2 is assumed to follow Michaelis–Menten kinetics,[14] where V_{max} and K_m represent the maximum reduction rate and Michaelis–Menten constant, respectively. All other reactions are assumed to follow the law of mass action and to proceed with a rate constant k_i in the forward direction and, if reversible within the time course of the study, with a rate constant k_{-i} in the reverse direction. The corresponding stoichiometric equations are also shown in Fig. 3.

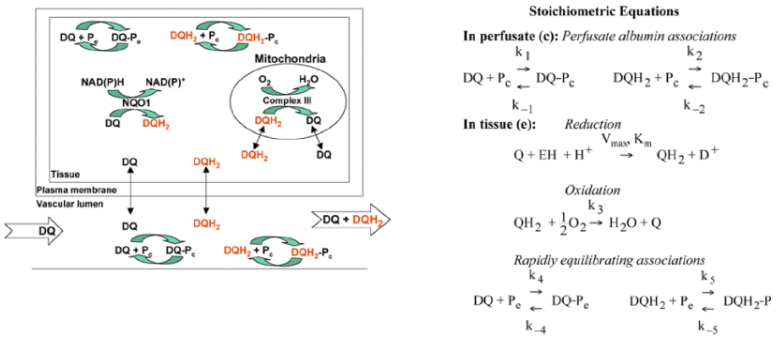

Fig. 3. Left: schematic illustration of the interactions occurring within the vasculature and the tissue as a bolus of DQ passes through the capillaries. Right: stoichiometric equations representing interactions shown on left.

Pulmonary capillary dimensions (diam=~5 μm and length=~1 mm[3]) are such that radial diffusion is sufficiently rapid to prevent radial indicator concentration gradients within the capillary lumen, even when the indicator extraction fraction is high. For instance, Bassingthwaighte et al.[34] estimated the time constant for radial diffusion in a 5-μm-diameter capillary with a radial diffusion coefficient of 10^{-5} cm/s to be ~6 ms, which is quite short when compared to pulmonary capillary transit times which range from one-half to several seconds.[35] On the other hand, the capillary length and magnitude of the Peclet number (ratio of convection to diffusion velocities) are such that mass transport by axial diffusion flux is not included within the capillary element model.[35,36]

The stoichiometric relationships can then be expressed by the following species balance equations, describing the spatial and temporal variations in FITC-dex (R), DQ, and DQH_2 within V_c and V_e :

Proceedings of the IEEE, Vol 94, No. 4 (April 2006): pg. 753-768. DOI.

$$\frac{\partial[R]}{\partial t} + W\frac{\partial[R]}{\partial x} = 0$$

$$\frac{\partial[\overline{\mathrm{DQ}}]}{\partial t} + W\left(\frac{V_c}{V_c + \frac{V_{F1}}{\alpha_1}}\right)\frac{\partial[\overline{\mathrm{DQ}}]}{\partial x} = \left(\frac{[\overline{\mathrm{DQH_2}}]}{V_c + \frac{V_{F1}}{\alpha_1}}\right)\left(\frac{k_o}{\alpha_3}\right) - \left(\frac{[\overline{\mathrm{DQ}}]}{V_c + \frac{V_{F1}}{\alpha_1}}\right) \times \left(\frac{V_{max}}{K_{\mathrm{ma}} + [\overline{\mathrm{DQ}}]}\right)$$

$$\frac{\partial[\overline{\mathrm{DQH_2}}]}{\partial t} + W\left(\frac{V_c}{V_c + \frac{V_{F2}}{\alpha_3}}\right)\frac{\partial[\overline{\mathrm{DQH_2}}]}{\partial x} = -\left(\frac{[\overline{\mathrm{DQH_2}}]}{V_c + \frac{V_{F2}}{\alpha_3}}\right)\left(\frac{k_o}{\alpha_3}\right) + \left(\frac{[\overline{\mathrm{DQ}}]}{V_c + \frac{V_{F2}}{\alpha_3}}\right) \times \left(\frac{V_{max}}{K_{\mathrm{ma}} + [\overline{\mathrm{DQ}}]}\right)$$

(1)(2)(3)

where $W = L/\overline{t}_c$ is the convective transport velocity and $\overline{t}_c$ is the capillary mean vascular transit time, and x=0 and x=L represent the capillary inlet and outlet, respectively. Indicator concentrations, at distance x from the capillary inlet at time t, of the total (free + bound) DQ and DQH_2 are represented by $[\overline{\mathrm{DQ}}]$ and $[\overline{\mathrm{DQH_2}}]$, respectively. Note that $[\overline{\mathrm{DQ}}] = [\mathrm{DQ}]\alpha_1$ and $[\overline{\mathrm{DQH_2}}] = ([\mathrm{DQH_2}]\alpha_3$, where $\alpha_1 = 1 + [P_c]k_1/k_{-1}$ and $\alpha_3 = 1 + [P_c]k_2/k_{-2}$ are constants accounting for the rapidly equilibrating interactions of DQ and DQH_2 with the perfusate. $K_{\mathrm{ma}} = \alpha_1 K_m(\mu\mathrm{M})$ is the apparent Michaelis–Menten constant; $V_{F1} = \alpha_2 V_e$ and $V_{F2} = \alpha_4 V_e$ (ml) are the virtual volumes of distribution, where $\alpha_2 = 1 + [P_e]k_4/k_{-4}$ and $\alpha_4 = 1 + [P_e]k_5/k_{-5}$ are constants accounting for the rapidly equilibrating interactions of

Proceedings of the IEEE, Vol 94, No. 4 (April 2006): pg. 753-768. DOI.

DQ and DQH_2 with lung tissue sites of association, respectively. Finally, $k_o = V_e k_3 [O_2]^{1/2} (ml \cdot \overset{-1}{min})$ is the tissue mediated DQH_2 oxidation rate constant. To put k_o in perspective, if one were to assume Michaelis–Menten kinetics for DQH_2 oxidation, k_o would be an approximation to the ratio of the maximum oxidation rate to the Michaelis–Menten constant. The $[H^+]$, $[O_2]$, and [EH] included in some parameter groups are assumed constant during a given sample collection period.[14]

Pulse infusion of DQ or DQH_2 corresponds to a steady-state model so that (1)–(3) reduce to

$$WV_c \frac{\partial[\overline{DQ}]}{\partial x} = [\overline{DQH_2}]\left(\frac{k_o}{\alpha_3}\right) - [\overline{DQ}]\left(\frac{V_{max}}{K_{ma} + [\overline{DQ}]}\right)$$

$$WV_c \frac{\partial[\overline{DQH_2}]}{\partial x} = -[\overline{DQH_2}]\left(\frac{k_o}{\alpha_3}\right) + [\overline{DQ}]\left(\frac{V_{max}}{K_{ma} + [\overline{DQ}]}\right). \quad (4)(5)$$

Given α_1 and α_3, the identifiable model parameters under steady-state conditions are the maximum reduction rate constant $V_{max}(\mu mol \cdot \overset{-1}{min})$; the apparent Michaelis–Menten constant, $K_{ma}(\mu M)$; and the tissue-mediated DQH_2 oxidation rate constant $k_o(ml \cdot \overset{-1}{min})$.

Under conditions of no oxidation of DQH_2 to DQ (i.e., $k_o = 0$), (4) and (5) simplify to the following uncoupled ordinary differential equations:

Proceedings of the IEEE, Vol 94, No. 4 (April 2006): pg. 753-768. DOI.

$$WV_c \frac{\partial[\overline{\mathrm{DQ}}]}{\partial x} = -[\overline{\mathrm{DQ}}]\left(\frac{V_{max}}{K_{\mathrm{ma}} + [\overline{\mathrm{DQ}}]}\right)$$

$$WV_c \frac{\partial[\overline{\mathrm{DQH_2}}]}{\partial x} = [\overline{\mathrm{DQ}}]\left(\frac{V_{max}}{K_{\mathrm{ma}} + [\overline{\mathrm{DQ}}]}\right).$$

(6)(7)

Equations (6) and (7) can be further simplified by assuming that all capillary pathways have the same transit time. Then integrating both sides of (6) results in (8), relating the rate of DQ reduction ν (μmol·min−1) to the steady-state venous outflow [DQ] and [DQH_2], V_{max}, and K_{ma}

$$\nu = \frac{V_{max}[\overline{\mathrm{DQ}}]_{\log}}{K_{\mathrm{ma}}[\overline{\mathrm{DQ}}]_{\log}}$$

(8)

where ν is the product of the outflow steady-state [DQH_2] during DQ infusion and the perfusate flow rate; and $\overline{\mathrm{DQ}}_{\log} = ([\mathrm{DQ}]_{\mathrm{in}} - [\mathrm{DQ}]_{\mathrm{out}})/\ln([\mathrm{DQ}]_{\mathrm{in}}/[\mathrm{DQ}]_{\mathrm{out}})$, where $[\mathrm{DQ}]_{\mathrm{in}}$ is outflow steady-state ($[\mathrm{DQ}] + [\mathrm{DQH_2}]$) and $[\mathrm{DQ}]_{\mathrm{out}}$ is outflow steady-state [DQ] during DQ infusion. $[\overline{\mathrm{DQ}}]_{\log}$, referred to as the log mean [DQ], is the effective [DQ] in the capillary region during DQ infusion, since [DQ] decreases as it passes through the capillaries.[14,37]

The kinetic parameters V_{max} and K_{ma} describing NQO_1-mediated DQ reduction can be estimated by fitting (8) to ν as a function of $[\overline{\mathrm{DQ}}]_{\log}$, as shown in Fig. 4 for normoxic and hyperoxic rat lungs. Given V_{max} and K_{ma}, the additional oxidation parameter was obtained by solving (4) and (5) and fitting the solution to data in Fig. 2.

Proceedings of the IEEE, Vol 94, No. 4 (April 2006): pg. 753-768. DOI.

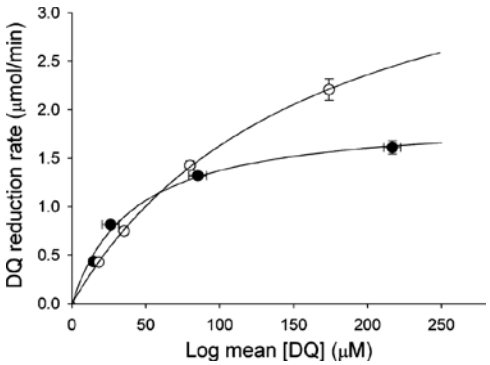

Fig. 4. DQ reduction rate versus log mean [DQ] during DQ infusion in the presence of cyanide (2 mM) in normoxic (n=4, filled circles) and hyperoxic (n=4, open circles) rat lungs. Values are mean ±SE. Solid lines are model fits to the data.

C. Redox Modeling Results

In the presence of cyanide, which inhibits tissue-mediated DQH_2 oxidation, the DQ reduction rate v is equal to the steady-state rate of DQH_2 outflow during DQ infusion. Fig. 4 shows v as a function of $[\overline{DQ}]_{log}$ for normoxic and hyperoxic lungs, where the solid lines correspond to the model fit of (8) to the data. Exposure to hyperoxia for 21 days significantly increased the estimates of both V_{max} (by ~110%) and K_{ma} (by ~240%) as compared to normoxic lungs.

The increase in Vmax is consistent with a hyperoxia-induced increase in lung NQO_1 activity in cells accessible to DQ on passage through hyperoxic lungs, presumably dominated by capillary endothelial cells.[14,15] The increase in K_{ma}, the Michaelis–Menten constant for DQ reduction, for hyperoxic lungs is not consistent with K_{ma} being an intensive property of the reductase. Since dicumarol inhibits other reductases,[38] one possible explanation for an increase in K_{ma} in hyperoxic lungs might be that other dicumarol-inhibitable DQ reductase(s) are induced.

Another possible explanation is an increase in the capillary transit time heterogeneity in hyperoxic lungs. The kinetic model described above assumes a homogeneous transit time distribution, i.e., all pathways have the same transit time. However, the relative dispersion of the vascular transit time distribution in hyperoxic lungs is ~40% greater than that of normoxic lungs. Since much of the vascular transit time heterogeneity occurs within the capillary bed,[14,35] an organ model which accounts for a heterogeneous distribution of capillary transit times $h_c(t)$ was used to evaluate the sensitivity of the estimates of V_{max} and K_{ma} on this heterogeneity. Model simulations revealed that V_{max} is virtually insensitive to $h_c(t)$, whereas K_{ma} is sensitive to an increase

Proceedings of the IEEE, Vol 94, No. 4 (April 2006): pg. 753-768. DOI.

in the heterogeneity of $h_c(t)$ which may account for the increased K_{ma} in hyperoxic lungs. These results suggest that knowledge of $h_c(t)$ may be important for reliable parameter estimation.

The role of endothelial cells in DQ reduction to DQH_2 on passage through the pulmonary circulation was confirmed using cultured pulmonary arterial endothelial cells. DQH2 was found to appear in the medium when cells were incubated with DQ, and dicumarol blocked the appearance of DQH_2. Furthermore, the estimated rate of DQ reduction, normalized to surface area, is on the same order as that estimated in rat lungs,[15] suggesting that the pulmonary endothelium is the dominant site of DQ reduction in the lungs. This is potentially important, since NQO_1 has been shown to confer protection from oxidant stress, and the pulmonary capillary endothelium is a primary site of O_2 toxicity.[31]

Section III.

Pulmonary Transit Time Distribution

The mean and distribution around the mean of blood transit or residence times within the pulmonary vasculature have important implications with regard to lung function. In particular, gas exchange between the alveolar air and blood, and substrate exchange between blood and tissue are dependent on, among other things, the pulmonary capillary transit times. The longer the capillary transit time, the more time available for exchange. Furthermore, it has been suggested that the rate of exchange is inversely proportional to the heterogeneity of the capillary transit time distribution $h_c(t)$ [39]. Thus, $h_c(t)$ is an important determinant of the overall efficiency of the exchange process, and plays an important role in the disposition of an indicator as it passes through the lungs.

In general, dispersion of a bolus within an organ occurs in: 1) conducting arteries and veins via velocity profile effects and heterogeneity of flows and/or lengths among parallel pathways and 2) the capillary bed due to its tortuous nature. The literature reveals that the whole spectrum of assumptions has been used, from all dispersion occurs within the arterial and venous trees so that the capillary transport function takes the form of a delta function, i.e., all capillaries have one common transit time,[40,41] to the assumption that the arterial and venous transport functions are delta functions so that all of the organ dispersion occurs within the capillary bed.[42,43] If the transit time dispersion within the arteries were due only to velocity profile effects, the bolus would be presented to all the capillaries at the same time, but it would be more dispersed than at the arterial input. Alternatively, if only heterogeneous transit times contributed to dispersion, each capillary

Proceedings of the IEEE, Vol 94, No. 4 (April 2006): pg. 753-768. DOI.

would receive an input concentration curve having no more dispersion than the original arterial input, but it would arrive at different capillaries at different times, resulting in an aggregated input to the entire capillary bed being more dispersed than the arterial input curve. Support for one of these alternatives, or a combination thereof, provides increased confidence in kinetic parameter estimates.

Determination of dispersion within different components of the vasculature begins with a mathematical formulation of the distribution of transit times through the total lung. The overall organ transit time distribution $h(t)$ can be regarded as a normalized frequency distribution of transit times whose shape depends on the flows and accessible volumes of each transit pathway through the organ. Similarly, the distribution of capillary transit times $h_c(t)$ represents the normalized frequency distribution of transit times through the pulmonary capillaries. In general, a transit time distribution is completely determined by knowledge of all of its moments μ^r about the mean μ, i.e.,

$$\mu^r = \int_0^\infty (t-\mu)^r h(t)dt$$

Assuming a linear, time-invariant system, the arterial inflow $c_I(t)$ and venous outflow $c_O(t)$ concentration curves can then be related using $c_O(t) = c_I(t) * h(t)$, where $*$ denotes temporal convolution, so that $h(t)$ can be determined using numerical deconvolution.[44] Alternatively, the moments of $h(t)$ can be calculated by taking the difference of the moments of $c_I(t)$ and $c_O(t)$, i.e., $\mu_h^r = \mu_o^r - \mu_I^r$. The same approach can be used in principle to determine $h_c(t)$ or its moments, except that $c_I(t)$ and $c_O(t)$ are interpreted as the arteriolar input and venule output of the capillary bed.

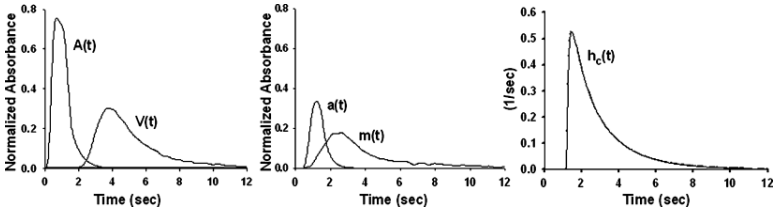

Fig. 5. Examples of data obtained from contrast-enhanced angiography of a rat lung. Left: pulmonary arterial inlet (A) and pulmonary venous outlet (V) Center: small artery (c_{in}, diam=200 μm) and microvasculature (m). Right: estimated capillary transit time distribution (h_c) obtained from c_{in}, and m using (11) and (12).

Proceedings of the IEEE, Vol 94, No. 4 (April 2006): pg. 753-768. DOI.

The contribution of the arterial and venous trees to the overall dispersion within the lung has been examined using contrast-enhanced x-ray angiography to image a bolus of contrast medium during its transit through the vasculature of a dog lung.[2] In this approach, the contrast medium serves as the vascular indicator so that indicator concentration curves were measured at the arterial inlet, the venous outlet, and selected locations within the intrapulmonary arterial and venous trees. Moment analysis was performed to estimate the moments of the overall lung $h(t)$ from the difference in the first and second moments (mean transit time and variance, respectively) of the inlet arterial and outlet venous curves. Also, moments at selected locations within the arterial were calculated and compared with those of the inlet artery curves to characterize the transit times and variances of arterial pathways. Transit times for the arterial pathways upstream from small arteries ($\sim$200 μm diam) were $\sim$20% of the total lung lobe transit time while the variance among these arterial transit times was less than $\sim$5% of the total variance of the lung. On average, the dispersion that occurred along a given arterial pathway was negligible. Since the venous results were similar, the study concluded that the arterial + venous mean transit time was $\sim$40% of the total mean transit time and the dispersion within the arterial and venous trees, as measured by their variances, was less than $\sim$20% of the total. Taken together, the results suggest that most of the heterogeneity in transit time in the intrapulmonary vasculature occurs within the pulmonary capillary bed rather than in conducting arteries or veins.[2]

Contrast-enhanced x-ray angiography was also used to deduce $h_c(t)$ by examining capillary regions within the images. Regional analysis was performed by acquiring a small inlet artery concentration curve $c_{\text{in}}(t)$ and regional capillary curve $m(t)$ proportional to the mass of contrast medium in the capillary region at time t. Examples in Fig. 5 were acquired from an isolated perfused rat lung during passage of a bolus of radiopaque contrast medium. Mass balance can be used to describe $m(t)$, i.e.,

$$m(t) = F \int_0^t [c_{\text{in}}(s) - c_{\text{out}}(s)]\, ds \tag{9}$$

where $c_{\text{in}}(t))$ and $c_{\text{out}}(t)$ are the capillary region inlet and outlet absorbance curves, respectively, and F is the constant flow rate through the capillary region.[45–46,47] By writing $c_{\text{out}}(t) = c_{\text{in}}(t) * h_c(t)$, (9) becomes

Proceedings of the IEEE, Vol 94, No. 4 (April 2006): pg. 753-768. DOI.

$$m(t) = Fc_{\text{in}}(t) * \left(1 - \int_0^t h_c(s)ds\right).$$

(10)

If we define

$$R_F(t) = F\left(1 - \int_0^t h_c(s)ds\right)$$

(11)

(10) becomes

$$m(t) = c_{\text{in}}(t) * R_F(t)$$

(12)

where the flow-weighted impulse residue function $R_F(t)$ represents $m(t)$ that would be measured if the inlet concentration curve were an impulse. The complete distribution of capillary transit times $h_c(t)$ can then be determined using numerical deconvolution [44]. Fig. 5 shows the estimate of $h_c(t)$ obtained for the capillary region of this rat lung example using this approach.

The above method requires measurement of inlet concentration curves from small arteries approaching the entrance to the capillary bed, such as those obtained via high magnification imaging. In the absence of these small artery curves, a modeling approach has been developed to estimate $h_c(t)$ from a vascular indicator and indicators that rapidly equilibrate between the blood and tissue on passage through the capillaries.[48,49] This method uses the notion that dispersion within the arteries and veins is the same for both types of indicators. However, in the capillaries, transit of rapidly equilibrating indicators is slowed due to the relatively larger volume of distribution. This delay depends on the capillary and tissue volumes as well as the tissue-to-plasma partition coefficient. Since the delay is distributed in proportion to the capillary transit time distribution for the vascular indicator, a fixed relationship between the moments of $h_c(t)$ of the vascular and rapidly equilibrating indicators can be determined. Knowing the moments, mean transit time,

Proceedings of the IEEE, Vol 94, No. 4 (April 2006): pg. 753-768. DOI.

variance, and skewness, say, a reasonable representation of $h_c(t)$ can be constructed using a random-walk or lagged-normal density function, for example.[44]

Section IV.

Modeling of Pulmonary Vascular Structure and Function

Continuous modulation of blood flow through vascular beds is paramount to the health of tissues, and ultimately the host organism in which they reside. Systemic control, managed by muscular arterioles and precapillary sphincters, has the task of providing a constant flow of blood through the tissues supplied by them, with little dependence on the mean arterial blood pressure. Control of the pulmonary circuit capillary flow is a different phenomenon in that muscular arterioles are absent and vascular control is exerted by muscular and partially muscular pulmonary arteries and veins. Compared to their systemic counterparts, normal pulmonary arteries are shorter and more distensible which gives them the capacity to accept high flow with little increase in pressure. In addition, under resting conditions, some capillaries do not conduct blood flow and are therefore recruitable under the demand of higher flow. In order for the pulmonary circulation to conduct the same volume as the entire systemic circulation with only a fraction of the driving force (~7 mmHg in the pulmonary compared to 90 mmHg in the systemic circulation of resting humans), pulmonary vascular resistance must be maintained at about one-fifteenth that of the systemic circulation and vary greatly to accept large swings in cardiac output.[50]

In the normal lung, the pulmonary arterial tree conducts high volumes of blood at low intraarterial pressure and helps to maintain the delicate balance between ventilation and perfusion. When there is persistent abnormally high blood pressure within the pulmonary vasculature, pulmonary hypertension is said to exist. Maladaptive changes in morphology due to disease and the accompanying pathophysiologic processes are referred to as remodeling.[9] In the lung, remodeling typically occurs in the parenchyma (e.g., fibrosis[51]), the airways (e.g., asthma[52]), and/or the vasculature (e.g., pulmonary arterial hypertension[53]). Pulmonary vascular remodeling, involving alteration of the composition and structure of the walls of the pulmonary vasculature, can be both a result of and cause of pulmonary hypertension. The walls of the muscular pulmonary arteries (greater than 30 μm diam) respond to chronic increases in intravascular pressure by becoming thicker and stronger, and neomuscularization occurs in precapillary pulmonary arteries normally void of muscle.[54] These changes, thought to be a compensatory response to protect vessels from leaks and aneurysms, can have a negative effect on the hemodynamics and gas exchange function of the lung. Although these may be useful adaptations to physiological stress,

Proceedings of the IEEE, Vol 94, No. 4 (April 2006): pg. 753-768. DOI.

under pathophysiological conditions they can result in detrimental effects on the lungs (higher resistance/impedance and/or decreased gas exchange) and heart (increased strain and hypertrophy).

Chronic exposure to low inspired oxygen levels (hypoxia) is an oxidative stress used as a common animal model of pulmonary hypertension.[5,55–56,57,58,59] An abundance of histological data on cellular composition, reactivity data from large isolated vessels, and changes in cellular metabolism in response to hypoxia and other models of pulmonary hypertension have been published.[53,55,56,59–60,61,62] However, complete understanding of the mechanisms and consequences of vascular remodeling requires knowledge of the etiology and impact of pulmonary hypertension on the longitudinal distribution of pulmonary vascular resistance, lumenal morphology, and branching patterns of the pulmonary arterial tree. Thus, mathematical models have been developed that integrate three-dimensional representations of the tree into the appropriate hemodynamic context to understand and predict flow and pressure distributions within the arterial tree.[4,63,64] These models can be used to predict the impact of pathologies, such as vessel drop out, decreased arterial distensibility, or both, to identify which treatment modalities are likely to have the most positive impact.

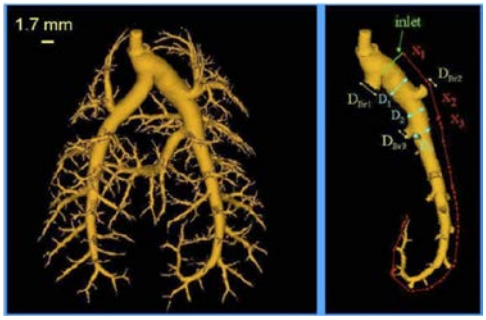

Fig. 6. Left: micro-CT surface shaded rendering of a normoxic rat pulmonary arterial tree. Right: rendering where the pulmonary arterial principal pathway has been identified. The location of the first several morphological measurements are indicated.

A. The Pulmonary Arterial Trunk

The pulmonary vascular tree has a complex branching structure, which is actually two adjacent trees (arterial and venous) that intricately connect at their most distal branches. For example, in humans, Horsfield measured 17 branching orders in the pulmonary arterial tree.[65] This implies the arterial network alone has on the order of 7.3×107 branches. Thus, measurement, or even modeling, of all vessels in the tree can be cumbersome. Since the spatial structure of the pulmonary arteries has been described as

Proceedings of the IEEE, Vol 94, No. 4 (April 2006): pg. 753-768. DOI.

fractal in nature.[10,66,67] it is prudent to use concepts related to fractal-like structures, such as self-consistency, to simplify data analysis and modeling calculations. To this end, the principal pathway was defined as the main pulmonary arterial trunk and its immediate daughter branches,[5,63,68,69] as shown in Fig. 6. A self-consistent tree has the property that the structure of all side branches off the principal pathway is statistically indistinguishable from their corresponding subregions of the main trunk. The subregion is that portion of the main trunk distal to the point at which the main trunk diameter equals the diameter of the side branch being compared. Thus, in a statistical sense, the principal pathway of a self-consistent tree would contain all of the information needed to rebuild the entire pulmonary arterial tree. Since rat pulmonary arterial trees have been shown to be self-consistent,[5,63,69] the task of measuring all the vessels in the pulmonary tree is reduced to measuring only the vessels along the main pulmonary trunk and the inlet diameter of its immediate daughter branches. Application of these simplifying conventions provides a means of summarizing the global morphometric and mechanical properties of the vascular tree from a reduced set of measurements.

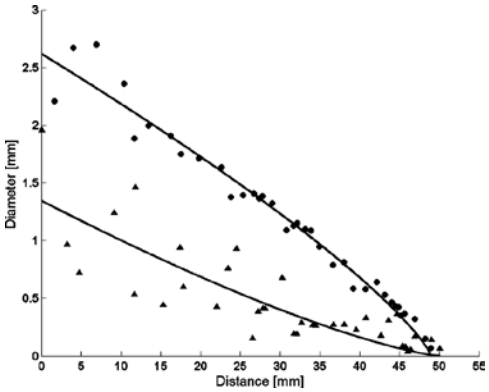

Fig. 7. Principal pathway data (main pulmonary arterial trunk, circles, and side daughter branches, triangles) from a normoxic rat lung. Pulmonary artery diameter D versus its distance x from the first lobar bifurcation as indicated by "inlet" in Fig. 6. The solid lines are the model fit of (13) and (14) to the data.

Sprague–Dawley rat lungs were imaged using micro-CT [69] at a constant airway pressure (6 mmHg) and a range of intravascular pressures (5.4, 12, 21, and 30 mmHg) following infusion of radiopaque contrast medium into the pulmonary arterial tree. Lengths and diameters of vessel segments along the main pulmonary trunk and each immediate daughter branch were measured from the reconstructed image volume acquired from a normoxic control rat and are shown in Fig. 7.

Proceedings of the IEEE, Vol 94, No. 4 (April 2006): pg. 753-768. DOI.

The geometric relationships along the principal pathway have been summarized using a mathematical model where diameter D of a vessel segment along the main trunk, at distance x from the inlet, is described by

$$D(x) = D(0)\left(1 - \frac{x}{Ltot}\right)^{c} \tag{13}$$

where $D(0)$ is the main trunk diameter at the first bifurcation (x=0), $Ltot$ is the total length of the main trunk, and c is a measure of the taper of the main trunk diameter from inlet to termination.[64,69] Similarly, the diameters of the side daughter branches can be described by

$$D_{\mathrm{Br}}(x) = D_{\mathrm{Br}}(0)\left(1 - \frac{x}{Ltot}\right)^{c_{\mathrm{Br}}} \tag{14}$$

where $D_{\mathrm{Br}}(0)$ is the diameter of the first daughter branch off the main trunk, i.e., the left pulmonary artery, and c_{Br} represents the taper of an equivalent trunk that could be created using the side daughter branches. The resulting model fit to the principal pathway and side daughter branch data are shown as the solid lines in Fig. 7.

Similarly, the relationship between the cumulative number of branches N_{Br} and distance along the main trunk, can be written as

$$N_{\mathrm{Br}}(x) = Ntot\left(1 - \left[1 - \left(\frac{x}{Ltot}\right)\right]\right)^{b} \tag{15}$$

where $Ntot$ is the total number of branches off the main trunk and b is a measure of how the branches are distributed along the vessel, i.e., when b>1, the number of branches per unit length increases with x and the opposite occurs when b<1. Fig. 8 shows branching data from the principal pathway measured in a normoxic rat lung and fit to model (15).

Proceedings of the IEEE, Vol 94, No. 4 (April 2006): pg. 753-768. DOI.

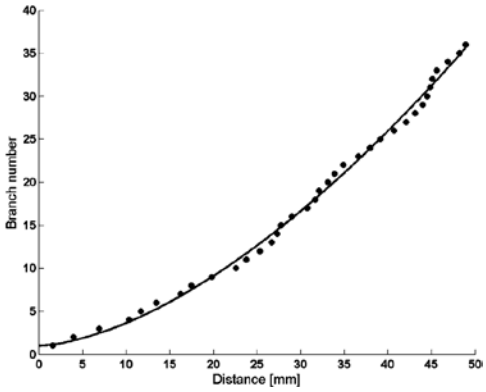

Fig. 8. Cumulative number of side branches N_{Br} versus distance x from the inlet from a normoxic rat lung (circles) and the model fit of (15) (solid line).

B. Structural and Biomechanical Effects of Vascular Remodeling

Common structural hallmarks of pulmonary vascular remodeling include artery lumenal narrowing, vessel wall thickening, and a decrease in the number of small arteries. In many rat models of pulmonary vascular remodeling, one of the first structural features observed is the appearance of neomuscularization of the small pulmonary arteries. This neomuscularization tends to increase pulmonary vascular resistance and decrease the number of parallel pathways, thereby diminishing excess capacitive volume in the vascular bed. Evidence of such changes can be observed visually in Fig. 9 as a reduction in background haze, corresponding to a potential loss in arterial density. These structural changes between normoxic and hypoxic rats are revealed quantitatively by parameters that estimate length of the pulmonary arterial main trunk ($Ltot = 44.1$mm and 39.9 mm for normoxia and hypoxia, respectively), and the number of branch orders ($Ntot = 36.4$ and 29.0 for normoxia and hypoxia, respectively).[5]

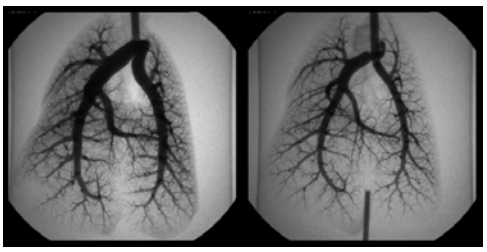

Fig. 9. X-ray projection image of contrast-filled normoxic (left) and hypoxic (right) rat lungs at a static vascular pressure=30 mmHg.

In addition to changes in structural parameters, the mechanical properties of remodeled vessels following exposure to chronic hypoxia have been investigated.[5] Vessel

wall thickening is frequently associated with stiffer vessels as measured by vessel distensibility. Arterial diameter D as a function of pressure P has been described by the relation

$$\frac{D(P)}{D_O} = 1 + \alpha P \tag{16}$$

where D_0 is arterial diameter at zero pressure, and α is referred to as "distensibility".[70] Equation (16) was fit to pressure and diameter data obtained from the CT images to evaluate the distensibility of individual vessels. This fitting revealed that α is nearly vessel-diameter independent, even for hypoxic rat lungs.[5,63,69] Thus, (16) was integrated into the principal pathway model using a single global α.[5] That is, (16) can be incorporated into (13) and (14) to obtain the more general model

$$D(x,P) = \quad D(0,0)(1+\alpha P)\left(1-\frac{x}{Ltot}\right)^{c}$$

$$D_{\mathrm{Br}}(x,P) = \quad D_{\mathrm{Br}}(0,0)(1+\alpha P)\left(1-\frac{x}{Ltot_{\mathrm{Br}}}\right)^{c_{\mathrm{Br}}}. \tag{17)(18}$$

Parameter estimates were obtained using the FMINUNC routine in the Matlab version 6.5, release 13, optimization toolbox by fitting (17) and (18) to the main trunk and side branch data measured from the control Sprague–Dawley rat lung at the four different intravascular pressures. The resulting parameter estimates were $D(0,0)$=1.42 mm and $Ltot$ = 49.0mm, c=0.78; $D_{\mathrm{Br}}(0,0)$ = 0.73mm and $Ltot_{\mathrm{Br}}$ = 49.0mm, c_{Br} = 1.35; and α=3.0% per mmHg. Fig. 10 shows these vessel measurement data and the corresponding surface generated from the fit using (17). Graphically, α represents the slope of the surface of the model fit to the principal pathway data over a range of intravascular pressures and diameters.

Proceedings of the IEEE, Vol 94, No. 4 (April 2006): pg. 753-768. DOI.

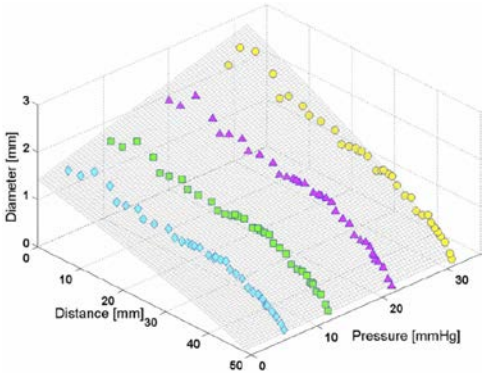

Fig. 10. Main trunk data from a normoxic rat lung plotted at vascular pressures of 5.4 (diamonds), 12 (squares), 21 (triangles), and 30 (circles) mmHg. Data symbols represent arterial diameter D as a function of vascular pressure P and distance from the inlet x. The surface represents the combined model fit to the principal pathway data as given in (17). The arterial distensibility α is reflected by the slope of the gray mesh surface with respect to pressure.

A previous study using this model revealed a significant decrease in arterial distensibility of hypoxic as compared to normoxic rats (2.8% per mmHg and 1.5% per mmHg for normoxia and hypoxia, respectively).[5] This twofold decrease in distensibility appears to be important because of its impact on the flow and pressure-volume distribution of blood in the pulmonary vasculature as described subsequently.

C. Functional Implications

As observed above, the mammalian pulmonary circulation is unique in that its primary function is to efficiently distribute blood flow to a dense interconnected capillary network in proportion to local alveolar ventilation, without precapillary sphincters. Instead, primary control of pulmonary blood flow, and thus, pulmonary blood pressure, is thought to be achieved primarily by flow partitioning via the connective structure of the pulmonary vessels as well as the vessel sizes, fine tuned by locally acting regulatory systems, e.g., pulmonary blood vessel constriction in response to alveolar hypoxia or dilation in response to stress-induced nitric oxide.[71] There is an extensive experimental literature devoted to the spatial distribution of pulmonary blood flow as well as alveolar ventilation and pulmonary perfusion matching, e.g.[11]

Various mathematical modeling studies have focused on understanding the impact of arterial network properties on the control of vascular pressure and flow in the pulmonary circulation.[6,72–73,74] Many of these studies have relied on morphometric data for the pulmonary arterial tree, i.e., the number, length, and diameter of pulmonary vessels and their connectivity, that exist in varying detail as statistical extrapolations of actual

Proceedings of the IEEE, Vol 94, No. 4 (April 2006): pg. 753-768. DOI.

morphometric measurements, e.g., Fig. 11.[6,72,73,75,76] Recently, Burrowes et al.[77] have begun to merge measurements providing detailed descriptions of the geometry of the large vessels obtained from volumetric CT, with statistically based models of the small-scale vascular structure. These studies have contributed significantly to the understanding of the flow distribution within the pulmonary circulation. As in most pulmonary blood flow modeling studies, Burrowes assumed steady laminar flow and rigid vascular structures. Although cardiac output, and hence pulmonary input, is pulsatile, their work, and other models that assume steady flow, is relevant because measurements of the pulmonary circulation indicate that the dominant component of pulmonary vascular impedance resides at the zero frequency.[78] Thus, in the pulmonary circulation model presented here, particularly for studies in which the pulmonary circulation is perfused with a constant pump flow, Occam's razor is employed[79] and pulmonary vessels are modeled using the assumption of steady flow in an idealized cylindrical blood vessel.

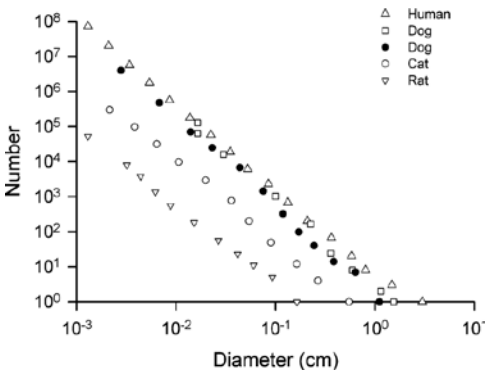

Fig. 11. Relationship between the number of vessels within a morphometric summary and mean arterial diameter from measurements on pulmonary arterial tree casts from human,[72] dog (squares,[73] and filled symbol,[6] cat,[69] and rat.[70]

Modeling begins by considering steady laminar flow F within a rigid cylindrical vessel with diameter D and length L. The pressure drop ΔP from the inlet to the outlet of the blood vessel is calculated using Poiseuilles's law, resulting in a fluid analog of Ohm's law $\Delta P = F \cdot R$, where the vessel acts as a "resistor" opposing the flow, with resistance R, given by

$$R = \frac{128\mu L}{\pi D^4} \tag{19}$$

and μ denotes fluid viscosity.[80] Under network topology assumptions involving the number and connective structure of the various size resistors (that is, the morphometric data), and ignoring additional losses due to the disruption of stream lines at bifurcations, the pulmonary vascular pressure, resistance, and flow computations translate into familiar Kirchoff current and voltage law calculations.[6,7,72–73,74,81]

Biomechanical properties of pulmonary arteries are thought to play an important role in determining the vascular pressure distribution within the lung. The extension of the concept of vascular resistance, (19), to idealized distensible vessels is discussed in Fung [80]. In Linehan et al.,[82] Fung's observations were employed using (16) to arrive at a nonlinear relationship between vessel flow (F), inlet pressure (P_a), outlet pressure (P_v), vessel distensibility (α), and resistance (R) corresponding to a rigid vascular geometry

$$P_a = \frac{[(1+\alpha P_v)^5 + 5\alpha RF]^{\frac{1}{5}} - 1}{\alpha}. \tag{20}$$

The relationship in (20) may be generalized, and at the same time simplified, by considering a nonlinear transformation of vascular pressure [4]. Let $D/D_0 = f(P)$, where $f(P)$ is a general function of pressure (e.g., the linear model of (16)). Denote a nonlinear transformation V, of pressure by $V(P) = \int (f(P))^4 dP$. For example, using (16), $V(P) = \int (1+\alpha P)^4 dP = (1+\alpha P)^5/\alpha$. If attention is focused on the transformed pressure variable, (20) becomes

$$\Delta V = V(P_a) - V(P_v) = RF. \tag{21}$$

Equation (21) then suggests that the upstream–downstream pressure difference ΔV in a distensible vessel is a fixed vascular resistance R, calculated using $D = D_0$ in (19), times vessel flow F. Equation (21) can be recognized as a form of "Ohm's Law," in which blood flow replaces current and V, transformed pressure, mimics the role of voltage.

As described above, both large and small pulmonary arteries in lungs of rats exposed to normoxia have distensibility that is well described by (16) with α=2.8% per mmHg independent of diameter, despite the fact that large and small pulmonary arteries exhibit different histological structure.[5] The hypoxic rat artery data was also well described by this model with α=1.5% per mmHg. With this in mind, (21) was

Proceedings of the IEEE, Vol 94, No. 4 (April 2006): pg. 753-768. DOI.

used to show that if a vascular tree were built such that each vessel had a common distensibility relationship $D/D_0 = f(P)$, then when a vessel experienced a fraction f of the total pulmonary arterial inflow at one inflow rate, the vessel would always experience the same fraction of total flow, regardless of whether the inflow rate (cardiac output) increased or decreased.[83] Such behavior would presumably be advantageous for the pulmonary vascular bed. In particular, once ventilation-perfusion matching was established, the connective structure and common distensibility would, without additional energy expenditures, aid in preserving perfusion without the need for an elaborate external control mechanism. Since exposure to hypoxia results in increased inlet pressures, we were interested in determining the impact of random perturbations in α on the terminal arterial flows. We also sought to determine whether the decrease in α observed with hypoxia would be sufficient to account for increased pulmonary arterial pressure, or whether rarefaction (i.e., a decrease in the number of vessels) suggested by the decrease in $Ntot$, $Ltot$ and the background haze in Fig. 9 might be required.

To begin to address this question, a previously described tree-growing algorithm[13] was used to simulate pulmonary arterial trees with different values of α. The longitudinal distribution of resistance from the inlet artery to the terminal arterioles was then examined for each tree. The simulated trees have the property that each vessel has a different size and the tree has a morphometric summary consistent with observed data, e.g., Fig. 11. However, the computer implementation was enhanced to account for vessel distensibility. Although each tree has the same number of total vessels, each vessel has a different zero-pressure diameter D_0, but the same D_0 is used in each tree; with the largest and smallest diameters being $D_0 = 1.6$ mm and 10 μm, respectively. Each individual pressure dependent diameter is given by (16). When a tree is first constructed, each vessel α is randomly selected according to a long cycle Gaussian pseudorandom number generator, with negative α discarded. Typical α distributions are shown in Fig. 12.

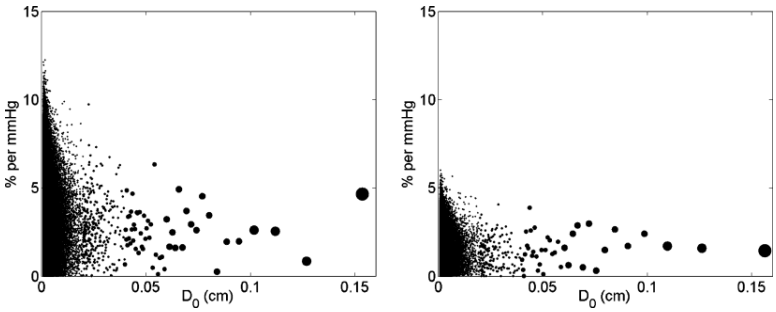

Fig. 12. Representative distensibility plots. Vertical axis is vessel distensibility α, in percent change per mmHg; horizontal axis is diameter, in cm, at zero pressure. $D_{max} = 1.6$mm, $D_{min} = 10\mu$m. Each symbol

Proceedings of the IEEE, Vol 94, No. 4 (April 2006): pg. 753-768. DOI.

represents one arterial segment, with symbol size modified to enhance visual interpretation. Left: mean α=2.8% per mmHg, CV=61% (normoxia). Right: α=1.5% per mmHg, CV=61% (hypoxia).

Since the rat pulmonary circulation exhibits a monopodial branching pattern, in order to report a longitudinal profile, a method of averaging the multitude of pathways is required. Previously we have reported vascular pressure as a function of cumulative vascular volume to all sites within the arterial tree that have the same pressure, that is, the total vascular volume that is upstream from a pressure isobar within the arterial tree.4,83 This manner of reporting vascular pressure as function of cumulative vascular volume is employed in Fig. 13. The panels of Fig. 13 show the average pressure-volume relationship obtained from five different arterial trees. Here each arterial tree consists of individual vessels modeled using an equal number of coupled nonlinear equations that are solved by successive iterations. The starting parameters are obtained using the rigid vessel resistance calculated using the D_0 to provide the initial pressure and vascular flow approximations. The outlet pressure at the terminal vessels of the arterial tree was fixed at 4 mmHg and the viscosity μ was 1.02 cP, appropriate for saline-perfused rat lungs. In both panels, the simulated normoxia trees consisted of 1 048 575 vessels and a distribution of α with mean 2.8% per mmHg and coefficient of variation 61%, resulting in pulmonary inlet pressures of 12.9 ± 0.1 mmHg (mean $\pm$ SE) and 18.6 ± 0.1 mmHg for inlet flows of 60 and 120 ml/min, respectively. In the left panel, the simulated hypoxic trees consisting of the same number of vessels with the same initial D_0 but with a distribution of α with mean 1.5% per mmHg, result in inlet pressures of 15.8 ± 0.1 and 23.9 ± 0.1 mmHg for inlet flows of 60 and 120 ml/min, respectively.

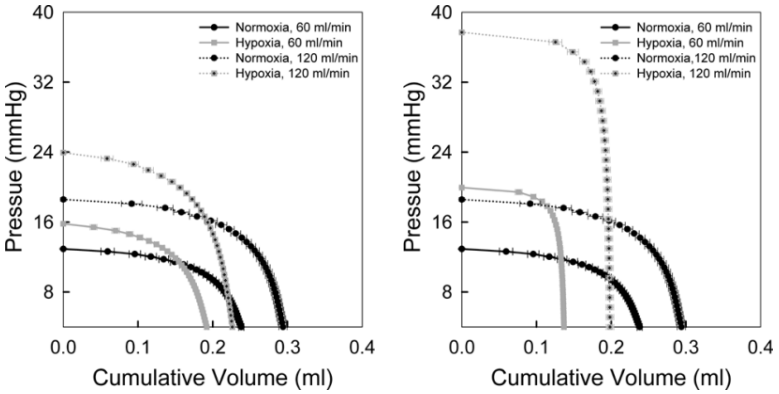

Fig. 13. Vascular pressure as a function of cumulative vascular volume. Lung inflow 60 ml/min (filled circles) or 120 ml/min (filled squares), outlet pressure 4 mmHg. Each symbol is mean and error bars are SE of 5 randomly created trees. Left: all trees consist of 1 048 575 vessels with $D = D_0(1 + \alpha P)$ and average α=1.5% (hypoxia) or 2.8% (normoxia) per mmHg. Right: Normoxic trees consist of 1 048 575

vessels with average α=2.8% per mmHg while hypoxic trees consist of 262 143 individual vessels with average α=1.5% per mmHg.

Although the lower α in the hypoxic trees resulted in higher pulmonary arterial pressure, this magnitude increase is not sufficient to account for the almost doubled arterial pressures observed in actual rat lungs after chronic hypoxic exposure. Thus, we investigated the possibility of rarefaction of vessels, as suggested by the decrease in $Ltot$ and $Ntot$ obtained from the micro-CT data and inspection of the change in background haze in the projection images (Fig. 9). The right panel of Fig. 13, shows the results from simulated hypoxic trees consisting of 262 143 individual vessels with a distribution of α with mean equal to 1.5% per mmHg and coefficient of variation of 61%. The decrease in parallel flow pathways resulted in increased mean pulmonary inlet pressures of 20.0 ± 0.1 and 37.7 ± 0.1 mmHg for inlet flows of 60 and 120 ml/min, respectively, which is consistent with pressures observed in hypoxic lungs. The longitudinal profiles in Fig. 13 suggest that, overall the pulmonary arterial tree may act as a pressure manifold, wherein most of the pressure drop is downstream near the terminals of the arterial tree.

In Fig. 14, the left and right panels represent the average normalized flow distribution from five simulated pulmonary arterial trees using normoxic and hypoxic parameters given above. In this setting, a normalized flow ratio is taken to be the flow in a terminal artery when pulmonary arterial tree inflow is 120 ml/min, divided by twice the flow in the same artery when pulmonary arterial tree inflow is 60 ml/min. The doubling of pulmonary arterial tree inflow was selected to simulate increased cardiac output, such as what might occur *in situ* with exercise in a rat. If no redistribution of flow occurred within the pulmonary arterial structures, all normalized flow ratios would be one. Thus, distributional deviations from one could be interpreted as a change in pulmonary vascular perfusion in response to a change in total flow. In constructing the random trees in Fig. 14, the outlet pressure for the arterial tree was again 4 mmHg and individual vessel distensibility given by (16). In the left panel, trees consisting of 1 048 575 vessels and average α=2.8% per mmHg were constructed to simulate normoxic trees, while in the right panel, trees consisting of 262 143 vessels and average α=1.5% per mmHg were constructed to simulate hypoxic remodeled trees. The increase in the spread of the flow distribution with hypoxia suggests that the capillary units see greater changes in fractional flow from control to hypoxia, which may have an impact on ventilation-perfusion matching. Extensive detailed data describing the redistribution of flow due to chronic exposure to hypoxia are not available, so that comparison of the model predictions to date is not yet possible. However, the model suggests that if rarefaction and vessel biomechanical properties change in the manner indicated, repartitioning of flow within the lung in

Proceedings of the IEEE, Vol 94, No. 4 (April 2006): pg. 753-768. DOI.

response to changes in cardiac output (e.g., as occurs with exercise) would potentially lead to changes in blood reoxygenation efficiency.

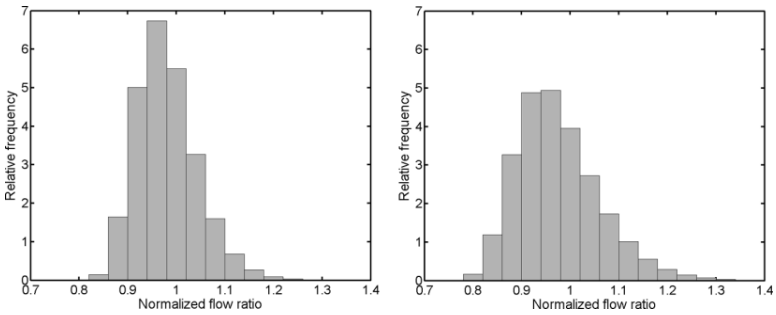

Fig. 14. Normalized terminal vessel flow ratio distributions. Each graph is the average of the distributions of five randomly constructed arterial trees, where normalized flow ratio is the flow in a terminal artery when lung inflow is 120 ml/min divided by twice the flow in the same artery at lung inflow of 60 ml/min. Tree outlet pressure 4 mmHg and individual vessel $D = D_0(1 + \alpha P)$. Left: Trees consist of 1 048 575 vessels and average α=2.8% per mmHg (normoxia). Right: trees consist of 262 143 vessels and average α=1.5% per mmHg (hypoxia).

Reeves et al., using a measurement methodology that provides a global estimate of pulmonary vessel distensibility, reported an initial baseline α=2.2% per mmHg in humans at sea level that, after three weeks at high altitude (6100 m) decreased to 0.8% per mmHg.[84] This change in α is in general agreement with those reported in normoxic and chronic hypoxia-exposed rats.[5] It is well known that hematocrit is elevated with chronic hypoxia exposure.[85] Increased hematocrit *in situ* may result in additional increases in vascular pressure; however, any change in viscosity due to increased hematocrit is not a factor in our simulations or experiments, since the isolated rat lungs are not perfused with blood.

Thus, overall the model suggests that a decrease in distensibility alone is insufficient to explain the increase in pressure associated with chronic hypoxia-induced pulmonary hypertension. Instead, the increase in pressure is better described when remodeling is characterized by both decreased distensibility and rarefaction of the vascular tree, although it may be that the increased pressure is due to lumenal narrowing. The use of mathematical modeling to distinguish amongst these hypotheses will require advances in experimentation, including additional high-resolution imaging to examine changes in the small arteries wherein much of the arterial resistance resides.[13]

Proceedings of the IEEE, Vol 94, No. 4 (April 2006): pg. 753-768. DOI.

Section V.

Conclusion

In summary, the lungs are well known for their gas exchange function. However, because the lungs have an endothelial surface approximately equal to that of the entire systemic circulation, and are situated between the systemic venous and arterial systems, they are well suited for their role of controlling not only arterial oxygen and carbon dioxide levels, but also other aspects of the chemical composition of the arterial blood. Thus, mathematical models of various forms have been developed as an aid in the investigation of the metabolic and hemodynamic functions of the lung.

Recent studies suggest that the pulmonary endothelium may modify the redox status of compounds during passage through the lung. Depending on the physical and chemical properties of the compound and the physiological status of the lungs, this potential redox modulation could result in regeneration of antioxidant capacity or production of pro-oxidant activity, which implies an important role for the lungs in maintenance of systemic vascular function. Indicator dilution methods and mathematical modeling have been used to begin to investigate these redox-active processes and the changes in their activity in response to oxidative stress.

Oxidative stress, resulting from hyperoxia, hypoxia or environmental toxins for example, may result in alterations to the lungs, including changes in the metabolic activity of the endothelium that potentially lead to vascular remodeling. In the case of animal exposure to a hypoxic environment, micro-CT data used in mathematical models and simulations have revealed that this remodeling is characterized by changes in the structural and biomechanical properties of the pulmonary vessels. In particular, the vessels become less distensible and the small vessels appear to narrow or perhaps even disappear. The impact of these changes on the flow and pressure distributions within the lung then has important implications for ventilation-perfusion matching and gas exchange in general.

A thorough mathematical/computational description of lung function will require models and data at all scales, from the genetic level up to the whole lung and beyond. For example, the recent work of Burrowes et al.[77,86] and Huang et al.[87] using computational fluid dynamics to describe blood transport within large and small pulmonary vessels has the potential to be incorporated into a global model of the lung circulatory system, along the lines suggested recently by Hunter and Nielsen.[79] Multiscale mathematical modeling

Proceedings of the IEEE, Vol 94, No. 4 (April 2006): pg. 753-768. DOI.

will undoubtedly play a key role in the integration of the emerging metabolic, hemodynamic, and morphometric databases.

References

[1]A. V. Clough, S. T. Haworth, W. Ma, C. A. Dawson, "Effects of hypoxia on pulmonary microvascular volume", *Amer. J. Physiol. Heart Circulat. Physiol.*, vol. 279, pp. H1274-H1282, 2000.

[2]A. V. Clough, S. T. Haworth, C. C. Hanger, J. Wang, D. L. Roerig, J. H. Linehan, C. A. Dawson, "Transit time dispersion in the pulmonary arterial tree", *J. Appl. Physiol.*, vol. 85, pp. 565-574, 1998.

[3]S. T. Haworth, J. H. Linehan, T. A. Bronikowski, C. A. Dawson, "A hemodynamic model representation of the dog lung", *J. Appl. Physiol.*, vol. 70, pp. 15-26, 1991.

[4]G. S. Krenz, C. A. Dawson, "Flow and pressure distributions in vascular networks consisting of distensible vessels", *Amer. J. Physiol. Heart Circulat. Physiol.*, vol. 284, pp. H2192-H2203, 2003.

[5]R. C. Molthen, K. L. Karau, C. A. Dawson, "Quantitative models of the rat pulmonary arterial tree morphometry applied to hypoxia-induced arterial remodeling", *J. Appl. Physiol.*, vol. 97, pp. 2372-2384, 2004.

[6]R. Z. Gan, R. T. Yen, "Vascular impedance analysis in dog lung with detailed morphometric and elasticity data", *J. Appl. Physiol.*, vol. 77, pp. 706-717, 1994.

[7]S. H. Bennett, B. W. Goetzman, J. M. Milstein, J. S. Pannu, "Role of arterial design on pulse wave reflection in a fractal pulmonary network", *J. Appl. Physiol.*, vol. 80, pp. 1033-1056, 1996.

[8]W. Mitzner, I. Huang, "Interpretation of pressure-flow curves in the pulmonary vascular bed" in *The Pulmonary Circulation in Health and Disease*, U.K., London:Academic, pp. 215-230, 1987.

[9]G. Selvetella, E. Hirsch, A. Notte, G. Tarone, G. Lembo, "Adaptive and maladaptive hypertrophic pathways: points of convergence and divergence", *Cardiovasc. Res.*, vol. 63, pp. 373-380, 2004.

[10]R. W. Glenny, H. T. Robertson, S. Yamashiro, J. B. Bassingthwaighte, "Applications of fractal analysis to physiology", *J. Appl. Physiol.*, vol. 70, pp. 2351-2367, 1991.

[11]M. P. Hlastala, R. W. Glenny, "Vascular structure determines pulmonary blood flow distribution", *News Physiol. Sci.*, vol. 14, pp. 182-186, 1999.

[12]C. A. Dawson, G. S. Krenz, K. L. Karau, S. T. Haworth, C. C. Hanger, J. H. Linehan, "Structure-function relationships in the pulmonary arterial tree", *J. Appl. Physiol.*, vol. 86, pp. 569-583, 1999.

[13]C. A. Dawson, G. S. Krenz, J. H. Linehan, "Complexity and structure-function relationships in the pulmonary arterial tree" in Lung Biology in Health and Disease: Complexity in Structure and Function of the Lung, New York:Marcel Dekker, pp. 401-427, 1998.

[14]S. H. Audi, R. D. Bongard, C. A. Dawson, D. Siegel, D. L. Roerig, M. P. Merker, "Duroquinone reduction during passage through the pulmonary circulation", *Amer. J. Physiol. Lung Cell Mol. Physiol.*, vol. 285, pp. L1116-L1131, 2003.

[15]M. P. Merker, R. D. Bongard, G. S. Krenz, H. Zhao, V. S. Fernandes, B. Kalyanaraman, N. Hogg, S. H. Audi, "Impact of pulmonary arterial endothelial cells on duroquinone redox status", *Free Radic. Biol. Med.*, vol. 37, pp. 86-103, 2004.

[16]C. A. Dawson, J. H. Linehan, D. A. Rickaby, T. A. Bronikowski, "Kinetics of serotonin uptake in the intact lung", *Ann. Biomed. Eng.*, vol. 15, pp. 217-227, 1987.

Proceedings of the IEEE, Vol 94, No. 4 (April 2006): pg. 753-768. DOI.

[17]S. H. Audi, D. L. Roerig, S. B. Ahlf, W. Lin, C. A. Dawson, "Pulmonary inflammation alters the lung disposition of lipophilic amine indicators", *J. Appl. Physiol.*, vol. 87, pp. 1831-1842, 1999.

[18]S. H. Audi, J. H. Linehan, G. S. Krenz, D. L. Roerig, S. B. Ahlf, C. A. Dawson, "Lipophilic amines as probes for measurement of lung capillary transport function and tissue composition using the multiple-indicator dilution method" in Whole Organ Approaches to Cellular Metabolism, New York:Springer-Verlag, pp. 517-543, 1998.

[19]J. H. Linehan, R. D. Bongard, D. L. Roerig, T. A. Bronikowski, C. A. Dawson, "Lung angiotensin-converting enzyme kinetics from indicator-dilution and constant-infusion methods", *Amer. J. Physiol.*, vol. 258, pp. H436-H444, 1990.

[20]M. P. Merker, I. M. Armitage, S. H. Audi, L. T. Kakalis, J. H. Linehan, J. R. Maehl, D. L. Roerig, C. A. Dawson, "Impact of angiotensin-converting enzyme substrate conformation on fractional hydrolysis in lung", *Amer. J. Physiol.*, vol. 270, pp. L251-L259, 1996.

[21]S. H. Audi, R. D. Bongard, Y. Okamoto, M. P. Merker, D. L. Roerig, C. A. Dawson, "Pulmonary reduction of an intravascular redox polymer", *Amer. J. Physiol. Lung Cell Mol. Physiol.*, vol. 280, pp. L1290-L1299, 2001.

[22]S. H. Audi, H. Zhao, R. D. Bongard, N. Hogg, N. J. Kettenhofen, B. Kalyanaraman, C. A. Dawson, M. P. Merker, "Pulmonary arterial endothelial cells affect the redox status of coenzyme Q0", *Free Radic. Biol. Med.*, vol. 34, pp. 892-907, 2003.

[23]S. H. Audi, C. A. Dawson, S. B. Ahlf, D. L. Roerig, "Lung tissue mitochondrial benzodiazepine receptors increase in a model of pulmonary inflammation", *Lung*, vol. 180, pp. 241-250, 2002.

[24]S. H. Audi, C. A. Dawson, S. B. Ahlf, D. L. Roerig, "Oxygen dependency of monoamine oxidase activity in the intact lung", *Amer. J. Physiol. Lung Cell Mol. Physiol.*, vol. 281, pp. L969-L981, 2001.

[25]D. L. Chen, M. A. Mintun, D. P. Schuster, "Comparison of methods to quantitate 18F-FDG uptake with PET during experimental acute lung injury", *J. Nucl. Med.*, vol. 45, pp. 1583-1590, 2004.

[26]D. P. Schuster, "The evaluation of lung function with PET", *Semin. Nucl. Med.*, vol. 28, pp. 341-351, 1998.

[27]A. B. Fisher, H. J. Forman, M. Glass, "Mechanisms of pulmonary oxygen toxicity", *Lung*, vol. 162, pp. 255-259, 1984.

[28]B. A. Freeman, J. D. Crapo, "Hyperoxia increases oxygen radical production in rat lungs and lung mitochondria", *J. Biol. Chem.*, vol. 256, pp. 10986-10992, 1981.

[29]L. L. Mantell, S. Horowitz, J. M. Davis, J. A. Kazzaz, "Hyperoxia-induced cell death in the lung—the correlation of apoptosis necrosis and inflammation", *Ann. NY Acad. Sci.*, vol. 887, pp. 171-180, 1999.

[30]J. M. Clark, C. J. Lambertsen, "Pulmonary oxygen toxicity: a review", *Pharmacol. Rev.*, vol. 23, pp. 37-133, 1971.

[31]J. D. Crapo, B. E. Barry, H. A. Foscue, J. Shelburne, "Structural and biochemical changes in rat lungs occurring during exposures to lethal and adaptive doses of oxygen", *Amer. Rev. Respir. Dis.*, vol. 122, pp. 123-143, 1980.

[32]Y. Wang, S. I. Feinstein, Y. Manevich, Y. S. Ho, A. B. Fisher, "Lung injury and mortality with hyperoxia are increased in peroxiredoxin 6 gene-targeted mice", *Free Radic. Biol. Med.*, vol. 37, pp. 1736-1743, 2004.

[33]J. D. Crapo, D. F. Tierney, "Superoxide dismutase and pulmonary oxygen toxicity", *Amer. J. Physiol.*, vol. 226, pp. 1401-1407, 1974.

[34]J. B. Bassingthwaighte, I. S. J. Chan, C. Y. Wang, "Computationally efficient algorithms for convection-permeation-diffusion models for blood-tissue exchange", *Ann. Biomed. Eng.*, vol. 20, pp. 687-725, 1992.

[35]S. H. Audi, J. H. Linehan, G. S. Krenz, C. A. Dawson, "Accounting for the heterogeneity of capillary transit times in modeling multiple indicator dilution data", *Ann. Biomed. Eng.*, vol. 26, pp. 914-930, 1998.

[36]L. Bass, P. J. Robinson, "Capillary permeability of heterogeneous organs: a parsimonious interpretation of indicator diffusion data", *Clin. Exp. Pharmacol. Physiol.*, vol. 9, pp. 363-388, 1982.

[37]L. Bass, P. J. Ribinson, "Effects of capillary heterogeneity on rates of steady uptake of substances by the intact liver", *Microvasc. Res.*, vol. 22, pp. 43-57, 1981.

[38]D. Ross, D. Siegel, H. Beall, A. S. Prakash, R. T. Mulcahy, N. W. Gibson, "DT-diaphorase in activation and detoxification of quinones. Bioreductive activation of mitomycin C", *Cancer Metastasis Rev.*, vol. 12, pp. 83-101, 1993.

[39]J. M. Gonzalez-Fernandez, S. E. Atta, "Maximal substrate transport in capillary networks", *Microvasc. Res.*, vol. 5, pp. 180-198, 1973.

[40]T. R. Harris, G. R. Bernard, K. L. Brigham, S. B. Higgins, J. E. Rinaldo, H. S. Borovetz, W. J. Sibbald, K. Kariman, C. L. Sprung, "Lung microvascular transport properties measured by multiple indicator dilution methods in patients with adult respiratory distress syndrome. A comparison between patients reversing respiratory failure and those failing to reverse", *Amer. Rev. Respir. Dis.*, vol. 141, pp. 272-280, 1990.

[41]T. R. Harris, K. L. Brigham, R. D. Rowlett, "Pressure serotonin and histamine effects on lung multiple-indicator curves in sheep", *J. Appl. Physiol.*, vol. 44, pp. 245-253, 1978.

[42]L. Jorfeldt, D. H. Lewis, J. B. Lofstrom, C. Post, "Lung uptake of lidocaine in healthy volunteers", *Acta Anaesthesiol. Scand.*, vol. 23, pp. 567-574, 1979.

[43]C. A. Goresky, W. H. Ziegler, G. G. Bach, "Capillary exchange modeling. Barrier-limited and flow-limited distribution", *Circulat. Res.*, vol. 27, pp. 739-764, 1970.

[44]A. V. Clough, D. Cui, J. H. Linehan, G. S. Krenz, C. A. Dawson, M. B. Maron, "Model-free numerical deconvolution of recirculating indicator concentration curves", *J. Appl. Physiol.*, vol. 74, pp. 1444-1453, 1993.

[45]J. T. Kuikka, J. B. Bassingthwaighte, M. M. Henrich, L. E. Feinendegen, "Mathematical modelling in nuclear medicine", *Eur. J. Nucl. Med.*, vol. 18, pp. 351-362, 1991.

[46]J. B. Bassingthwaighte, "Microcirculatory considerations in NMR flow imaging", *Magn. Reson. Med.*, vol. 14, pp. 172-178, 1990.

[47]A. V. Clough, A. Al-Tinawi, J. H. Linehan, C. A. Dawson, "Regional transit time estimation from image residue curves", *Ann. Biomed. Eng.*, vol. 22, pp. 128-143, 1994.

[48]S. H. Audi, G. S. Krenz, J. H. Linehan, D. A. Rickaby, C. A. Dawson, "Pulmonary capillary transport function from flow-limited indicators", *J. Appl. Physiol.*, vol. 77, pp. 332-351, 1994.

[49]S. H. Audi, J. H. Linehan, G. S. Krenz, C. A. Dawson, S. B. Ahlf, D. L. Roerig, "Estimation of the pulmonary capillary transport function in isolated rabbit lungs", *J. Appl. Physiol.*, vol. 78, pp. 1004-1014, 1995.

[50]R. L. Vick, Contemporary Medical Physiology, CA, Menlo Park:Addison-Wesley, 1979.

[51]K. Kuwano, N. Hagimoto, Y. Nakanishi, "The role of apoptosis in pulmonary fibrosis", *Histol. Histopathol.*, vol. 19, pp. 867-881, 2004.

Proceedings of the IEEE, Vol 94, No. 4 (April 2006): pg. 753-768. DOI.

[52]F. H. Chen, K. T. Samson, K. Miura, K. Ueno, Y. Odajima, T. Shougo, Y. Yoshitsugu, S. Shioda, "Airway remodeling: A comparison between fatal and nonfatal asthma", *J. Asthma*, vol. 41, pp. 631-638, 2004.

[53]K. R. Stenmark, R. P. Mecham, "Cellular and molecular mechanisms of pulmonary vascular remodeling", *Annu. Rev. Physiol.*, vol. 59, pp. 89-144, 1997.

[54]J. Hughes, N. Morrell, "Pulmonary vascular remodeling" in Pulmonary Circulation: From Basic Mechanisms to Clinical Practice, U.K., London:Imperial College, pp. 71-85, 2001.

[55]A. Hislop, L. Reid, "New findings in pulmonary arteries of rats with hypoxia-induced pulmonary hypertension", *Br. J. Exp. Pathol.*, vol. 57, pp. 542-554, 1976.

[56]T. K. Jeffery, N. W. Morrell, "Molecular and cellular basis of pulmonary vascular remodeling in pulmonary hypertension", *Prog. Cardiovasc. Dis.*, vol. 45, pp. 173-202, 2002.

[57]M. Rabinovitch, W. Gamble, A. S. Nadas, O. S. Miettinen, L. Reid, "Rat pulmonary circulation after chronic hypoxia: hemodynamic and structural features", *Amer. J. Physiol.*, vol. 236, pp. H818-H827, 1979.

[58]R. J. van Suylen, J. F. Smits, M. J. Daemen, "Pulmonary artery remodeling differs in hypoxia- and monocrotaline-induced pulmonary hypertension", *Amer. J. Resp Crit Care Med.*, vol. 157, pp. 1423-1428, 1998.

[59]B. Meyrick, L. Reid, "Hypoxia-induced structural changes in the media and adventitia of the rat hilar pulmonary artery and their regression", *Amer. J. Path.*, vol. 100, pp. 151-178, 1980.

[60]B. Meyrick, L. Reid, "Development of pulmonary arterial changes in rats fed Crotalaria spectabilis", *Amer. J. Path.*, vol. 94, pp. 37-51, 1979.

[61]C. J. Emery, G. Q. Teng, X. Liu, G. R. Barer, "Vasoreactions to acute hypoxia whole lungs and isolated vessels compared: modulation by NO", *Respir. Physiol. Neurobiol.*, vol. 134, pp. 115-129, 2003.

[62]J. A. Madden, P. A. Keller, R. M. Effros, C. Seavitte, J. S. Choy, A. D. Hacker, "Responses to pressure and vasoactive agents by isolated pulmonary arteries from monocrotaline-treated rats", *J. Appl. Physiol.*, vol. 76, pp. 1589-1593, 1994.

[63]K. L. Karau, R. C. Molthen, A. Dhyani, S. T. Haworth, C. C. Hanger, D. L. Roerig, R. H. Johnson, C. A. Dawson, "Pulmonary arterial morphometry from microfocal X-ray computed tomography", *Amer. J. Physiol. Heart Circulat. Physiol.*, vol. 281, pp. H2747-H2756, 2001.

[64]R. C. Molthen, K. L. Karau, C. A. Dawson, "Quantitative models of the rat pulmonary arterial tree morphometry applied to hypoxia-induced arterial remodeling", *J. Appl. Physiol.*, vol. 97, pp. 2372-2384, 2004.

[65]K. Horsfield, "Functional morphology of the pulmonary vasculature" in Respiratory Physiology: An Analytical Approach, New York:Marcel Dekker, Inc., vol. 40, pp. 499-531, 1989.

[66]L. M. Boxt, J. Katz, L. S. Liebovitch, R. Jones, P. D. Esser, L. Reid, "Fractal analysis of pulmonary arteries: the fractal dimension is lower in pulmonary hypertension", *J. Thorac. Imaging*, vol. 9, pp. 8-13, 1994.

[67]M. Zamir, "On fractal properties of arterial trees", *J. Theor Biol.*, vol. 197, pp. 517-526, 1999.

[68]J. J. Fredberg, A. Hoenig, "Mechanical response of the lungs at high frequencies", *J. Biomech Eng.*, vol. 100, pp. 57-66, 1978.

[69]K. L. Karau, R. H. Johnson, R. C. Molthen, A. H. Dhyani, S. T. Haworth, C. C. Hanger, D. L. Roerig, C. A. Dawson, "Microfocal X-ray CT imaging and pulmonary arterial distensibility in excised rat lungs", *Amer. J. Physiol. Heart Circulat. Physiol.*, vol. 281, pp. H1447-H1457, 2001.

Proceedings of the IEEE, Vol 94, No. 4 (April 2006): pg. 753-768. DOI.

[70]A. Al-Tinawi, G. S. Krenz, D. A. Rickaby, J. H. Linehan, C. A. Dawson, "Influence of hypoxia and serotonin on small pulmonary vessels", *J. Appl. Physiol.*, vol. 76, pp. 56-64, 1994.

[71]M. S. Goligorsky, H. Li, S. Brodsky, J. Chen, "Relationships between caveolae and eNOS: everything in proximity and the proximity of everything", *Amer. J. Physiol. Renal Physiol.*, vol. 283, pp. F1-F10, 2002.

[72]R. T. Yen, F. Y. Zhuang, Y. C. Fung, H. H. Ho, H. Tremer, S. S. Sobin, "Morphometry of cat's pulmonary arterial tree", *J. Biomech Eng.*, vol. 106, pp. 131-136, 1984.

[73]Z. L. Jiang, G. S. Kassab, Y. C. Fung, "Diameter-defined Strahler system and connectivity matrix of the pulmonary arterial tree", *J. Appl. Physiol.*, vol. 76, pp. 882-892, 1994.

[74]G. S. Krenz, J. H. Linehan, C. A. Dawson, "A fractal continuum model of the pulmonary arterial tree", *J. Appl. Physiol.*, vol. 72, pp. 2225-2237, 1992.

[75]K. Horsfield, "Morphometry of the small pulmonary arteries in man", *Circulat. Res.*, vol. 42, pp. 593-597, 1978.

[76]W. S. Miller, "The structure of the lung", *J. Morphol.*, vol. 8, pp. 165-182, 1893.

[77]K. S. Burrowes, P. J. Hunter, M. H. Tawhai, "Anatomically based finite element models of the human pulmonary arterial and venous trees including supernumerary vessels", *J. Appl. Physiol.*, vol. 99, pp. 731-738, 2005.

[78]W. W. Nichols, M. F. O'Rouke, McDonald's Blood Flow in Arteries: Theoretical Experimental and Clinical Principles, London:Hodder Arnold, 2005.

[79]P. Hunter, P. Nielsen, "A strategy for integrative computational physiology", *Physiology*, vol. 20, pp. 316-325, 2005.

[80]Y. C. Fung, *Biomechanics: Circulation*, 1997.

[81]J. Zhang, C. A. Piantadosi, "Prevention of H_2O_2 generation by monoamine oxidase protects against CNS O_2 toxicity", *J. Appl. Physiol.*, vol. 71, pp. 1057-1061, 1991.

[82]J. H. Linehan, S. T. Haworth, L. D. Nelin, G. S. Krenz, C. A. Dawson, "A simple distensible vessel model for interpreting pulmonary vascular pressure-flow curves", *J. Appl. Physiol.*, vol. 73, pp. 987-994, 1992.

[83]G. S. Krenz, C. A. Dawson, "Vessel distensibility and flow distribution in vascular trees", *J. Math Biol.*, vol. 44, pp. 360-374, 2002.

[84]J. T. Reeves, J. H. Linehan, K. R. Stenmark, "Distensibility of the normal human lung circulation during exercise", *Amer. J. Physiol. Lung Cell Mol. Physiol.*, vol. 288, pp. L419-L425, 2005.

[85]R. D. Petit, R. R. Warburton, L. C. Ou, N. S. Hill, "Pulmonary vascular adaptations to augmented polycythemia during chronic hypoxia", *J. Appl. Physiol.*, vol. 79, pp. 229-235, 1995.

[86]K. S. Burrowes, M. H. Tawhai, P. J. Hunter, "Modeling RBC and neutrophil distribution through an anatomically based pulmonary capillary network", *Ann. Biomed. Eng.*, vol. 32, pp. 585-595, 2004.

[87]Y. Huang, C. M. Doerschuk, R. D. Kamm, "Computational modeling of RBC and neutrophil transit through the pulmonary capillaries", *J. Appl. Physiol.*, vol. 90, pp. 545-564, 2001.